Grain size dependence of the twin length fraction in nanocrystalline Cu thin films via transmission electron microscopy based orientation mapping

Xuan Liu and Noel T. Nuhfer
Department of Materials Science and Engineering, Carnegie Mellon University, Pittsburgh, Pennsylvania 15213, USA

Andrew P. Warren and Kevin R. Coffey
Department of Materials Science and Engineering, University of Central Florida, Orlando, Florida 32816, USA

Gregory S. Rohrer
Department of Materials Science and Engineering, Carnegie Mellon University, Pittsburgh, Pennsylvania 15213, USA

Katayun Barmak[a)]
Department of Applied Physics and Applied Mathematics, Columbia University, New York, NY 10027, USA

(Received 8 July 2014; accepted 1 December 2014)

Transmission electron microscopy (TEM) based orientation mapping has been used to measure the length fraction of coherent and incoherent Σ3 grain boundaries in a series of six nanocrystalline Cu thin films with thicknesses in the range of 26–111 nm and grain sizes from 51 to 315 nm. The films were annealed at the same temperature (600 °C) for the same length of time (30 min), have random texture, and vary only in grain size and film thickness. A strong grain size dependence of Σ3 (coherent and incoherent) and coherent Σ3 boundary fraction was observed. The experimental results are quantitatively compared with three physical models for the formation of annealing twins developed for microscale materials. The experimental results for the nanoscale Cu films are found to be in good agreement with the two microscale models that explain twin formation as a growth accident process.

I. INTRODUCTION

Properties of materials, such as electrical resistivity,[1,2] corrosion resistance,[3] and dielectric phenomena,[4] are strongly influenced by the type of grain boundaries in the material and how they are connected. The concept of grain boundary design (now known as grain boundary engineering) was first proposed by Watanabe.[5] Grain boundary engineering aims to increase the fraction of special grain boundaries with desirable properties.[6] Desirable properties can often be associated with boundaries with simple structures and low energy. Such low-energy structures are, in turn, associated with coincident site lattice (CSL) boundaries.[7] Twin boundaries are a type of CSL boundary (noted as Σ3) and are commonly found in face centered cubic (fcc) materials with medium to low stacking fault energies, as is the case for Cu. Crystals separated by Σ3 twin boundaries are misoriented by a 60° rotation about a common <111> axis. A Σ3 twin boundary is classified as coherent when the boundary is in the {111} plane perpendicular to the misorientation axis and as incoherent otherwise. Properties of coherent and incoherent Σ3 grain boundaries can be significantly different, including the reflection coefficients for electron scattering.[8]

In recent years, extensive research has been focused on the effect of twin boundaries on the properties of Cu.[9–13] For example, Shen et al.[9] showed that a high density of twin boundaries in ultrafine grained Cu results in high tensile strength while retaining significant ductility. In the work by Anderoglu et al.,[10] sputtered Cu films with a layered arrangement of coherent twin boundaries exhibited better thermal stability than crystals without these boundaries. Twin boundaries are also thought to have little impact on resistivity[12] and to enhance the electromigration resistance[11,13] of Cu.

Motivated by the various desirable properties resulting from the presence of twin boundaries, efforts have been made to study the influence of microstructure and processing conditions on twin formation in Cu. Kohama et al.[14] investigated the role of texture in grain growth and twin boundary formation in Cu films. A strong (111) texture was observed to suppress grain growth and twin boundary formation, while a (100) texture facilitated the same processes. Park and Field[15] found a dependence of twin boundary formation on annealing temperature and

Contributing Editor: Robert C. Cammarata
[a)]Address all correspondence to this author.
e-mail: kb2612@columbia.edu
DOI: 10.1557/jmr.2014.393

film thickness in three sputter deposited Cu films with thicknesses of 100, 480, and 850 nm. Pantleon et al.[16] studied three micrometer thick self-annealed Cu films and found an increase in average grain size and Σ3 boundary density with film thickness.

In this work, a TEM based orientation mapping technique called ASTAR™ is used to measure the length fraction of Σ3 grain boundaries in Cu films with nanometer scale thicknesses well below the range studied in prior works. The Σ3 length fraction is the result of a two-dimensional analysis that assigns Σ3 boundaries as twins if the surface trace is consistent with the boundary terminating on a (111) plane. The density of Σ3 boundaries is also evaluated by the peak intensity of the Σ3 boundary area using an established stereological measurement method. A detailed description of the crystal orientation mapping system can be found in earlier publications.[17–19] ASTAR™ has been successfully used to study heterophase interface character and grain boundary character distributions in nanocrystalline materials.[20–22] In the work by Carpenter et al. and Liu et al.,[21–23] the heterophase interfacial texture of Cu/Nb nanolamellar composites with average layer thicknesses as small as 18 nm was explored. Comparisons with bulk texture measurements provided by neutron diffraction demonstrated that the orientation mapping results were representative of bulk textures in both the Cu and Nb phases.[21] In the work by Liu et al.,[24] crystal orientation maps were obtained of a nanocrystalline tungsten thin film with a 100 nm average grain size wherein the distribution of grain boundary planes at specific lattice misorientations was obtained and was compared with the populations of the same boundaries in a microcrystalline ferritic steel. When the grain boundary character distributions (GBCDs) of the two materials were compared, it was found that they were correlated, so that the most common boundaries in tungsten were also the most common boundaries in ferrite steel. Darbal et al.[20] studied the GBCDs of two Cu thin films with average layer thicknesses of 36.9 and 46.4 nm based on crystal orientation maps. The two Cu films showed strong peaks in the GBCD at the coherent Σ3 position.

Various attempts have been made to describe the formation and growth of twin boundaries in fcc materials. The most well-known models invoke the occurrence of growth accidents,[25,26] grain encounters,[27–29] stacking fault packets,[30] grain boundary dissociation,[31,32] or other nonspecific mechanisms.[33] Details about each model will be given in the Discussion section. However, in this paper, we will focus on models that lend themselves to quantitative comparison with our experimental results.

\The purpose of the current paper is to present measurements of the Σ3 and coherent Σ3 boundary length fractions in a series of six Cu thin films encapsulated by $Ta_{38}Si_{14}N_{48}$ layers. The deposition conditions and annealing temperature were such that all films have a random texture and a microstructure consisting of a single grain through the film thickness. There are three major novelties of the work. First, compared with most previous work, a larger number of Cu films with different thicknesses were studied. This allows a systematic comparison between the measured twin fraction and fractions calculated from existing physical models. Secondly, all films studied in this work have nanometer scale film thicknesses (26–111 nm) and grain sizes (51–315 nm). This scale is of significant interest in many current applications.[34] Finally, all of the samples had exactly the same thermal treatment and vary only in their grain size and thickness. As the film thickness is not considered to be an influential factor for twin density in any existing physical models, it is neglected in favor of grain size in comparing the experimental work with models of twin formation. Therefore, this experiment separates the influence of grain size from thermal treatment and allows a more rigorous comparison to established twin formation models than possible in typical grain growth experiments.

II. EXPERIMENTAL

A. Film processing

The six Cu films examined in this work were sputter deposited onto (100) Si substrates having a 150 nm thick layer of thermally grown SiO_2 and were encapsulated between 20 nm of SiO_2 and 2 nm of $Ta_{38}Si_{14}N_{48}$ to form a Si/thermal SiO_2/sputtered SiO_2/$Ta_{38}Si_{14}N_{48}$/Cu/$Ta_{38}Si_{14}N_{48}$/sputtered SiO_2 layer structure. The substrate was cooled to −40 °C by contact with a liquid nitrogen cooled Cu plate. The Cu layers were deposited by dc sputter deposition from high-purity (99.9999%) Cu targets. The deposited films had thicknesses in the range of 25.6–111.1 nm, measured by x-ray reflectivity at the Stanford Synchrotron Radiation Lightsource. Following deposition, the films were postannealed at 600 °C for 30 min in Ar + 3% H_2 to achieve a columnar grain structure. Cross-sectional TEM micrographs of the film with a Cu layer thickness of 56.8 nm are shown in Figs. 1(a) and 1(b). Details of film deposition and processing of similar sets of Cu thin films can be found elsewhere.[1,35]

Plan-view TEM samples were prepared by first removing most of the Si by mechanical polishing from the back side and then etching in a mixture of HF and HNO_3.[36] The etching was stopped before breaking into the Cu film, resulting in large-area, uniformly thick, electron transparent samples for TEM.

B. TEM characterization and orientation mapping

Void fractions of the films were measured using high-angle annular dark field (HAADF) imaging in the

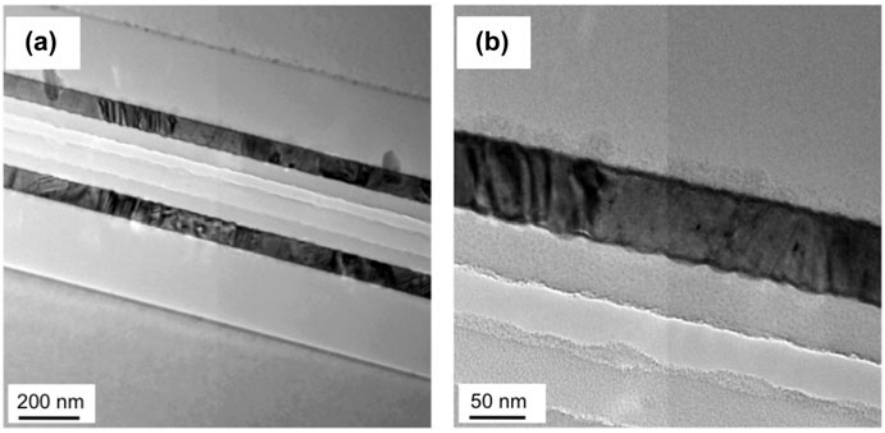

FIG. 1. Cross-sectional TEM micrograph of the Cu film with a thickness of 56.8 nm at two different magnifications.

scanning transmission electron microscopy mode. Measured void fractions of the six Cu films are shown in Table I and are seen to be in the range of 0.7–1.4%, with the highest void fraction of 1.4% found in the thinnest film. Given the low void fraction of the films, very few of the grains neighbor a void or could be affected by a void and the films can therefore be considered to behave as continuous.

Orientation imaging was performed on an ASTAR™ (NanoMEGAS, Brussels, Belgium) system installed on a FEI Tecnai F20 TEM (FEI Corporation, Hillsboro, OR) with a field emission gun and an accelerating voltage of 200 kV. A probe size of 9 in the FEI Tecnai F20, which corresponds to a beam diameter of ~1 nm, was used for collection of orientation maps. A condenser aperture with a diameter of 30 μm was used. Scan step sizes were chosen to be roughly consistent with the corresponding estimated grain sizes excluding twin boundaries and ranged between 2.5 and 12.5 nm for all six samples. The influence of step size on twin boundary length fraction measurements is discussed in Sec. III. D. Each orientation map contains 250–300 steps along both x and y directions. Approximately 30 fields of views with ~100–200 grains in each field of view were collected and used for both grain size measurement and Σ3 boundary length fraction measurement. Detailed scan parameters used for each sample can be found in Table II. Example orientation maps of the six films are given in Fig. 2.

For the determination of grain boundary character distribution, the ASTAR™ orientation data were rotated counterclockwise by 207° to bring the image and diffraction pattern orientations into coincidence. The ASTAR™ orientation data were then imported into the TSL OIM™ software (EDAX, Mahwah, NJ) for analysis. An additional counterclockwise rotation of 90° was applied to correct the difference in the reference frames between ASTAR™ and TSL.[20]

TABLE I. Void fractions of the six Cu films measured by HAADF.

Thickness (nm)	Void fraction (%)
25.6	1.4
38.2	1.1
39.4	1.0
56.8	0.9
72.4	0.7
111.1	0.7

TABLE II. Scan parameters used for each Cu sample.

Cu layer thickness (nm)	Scan step size (nm)	No. of steps
25.6	2.5	300
38.2	2.5	300
39.4	5	250
56.8	7	250
72.4	7.5	250
111.1	12.5	250

C. Cleanup of orientation data using TSL OIM™

Data cleanup needs to be applied to orientation data for removal of incorrectly indexed data points, especially near grain boundaries. First, a grain dilation filter is used which acts only on points which do not belong to any defined grain. The points will become part of the grain with the largest number of pixels surrounding the pixel of interest. Two parameters need to be defined for the grain dilation filter, the minimum grain size and the misorientation angle. For the Cu films studied here, the misorientation angle is defined to be 5°, thus neighboring pixels misoriented by less than 5° are considered to belong to the same grain. The minimum grain size is defined to be 5% of the mean grain area excluding twin boundaries, estimated from the uncleaned orientation maps.

After grain dilation, the single orientation per grain operation with a tolerance angle of 5° is used to assign an

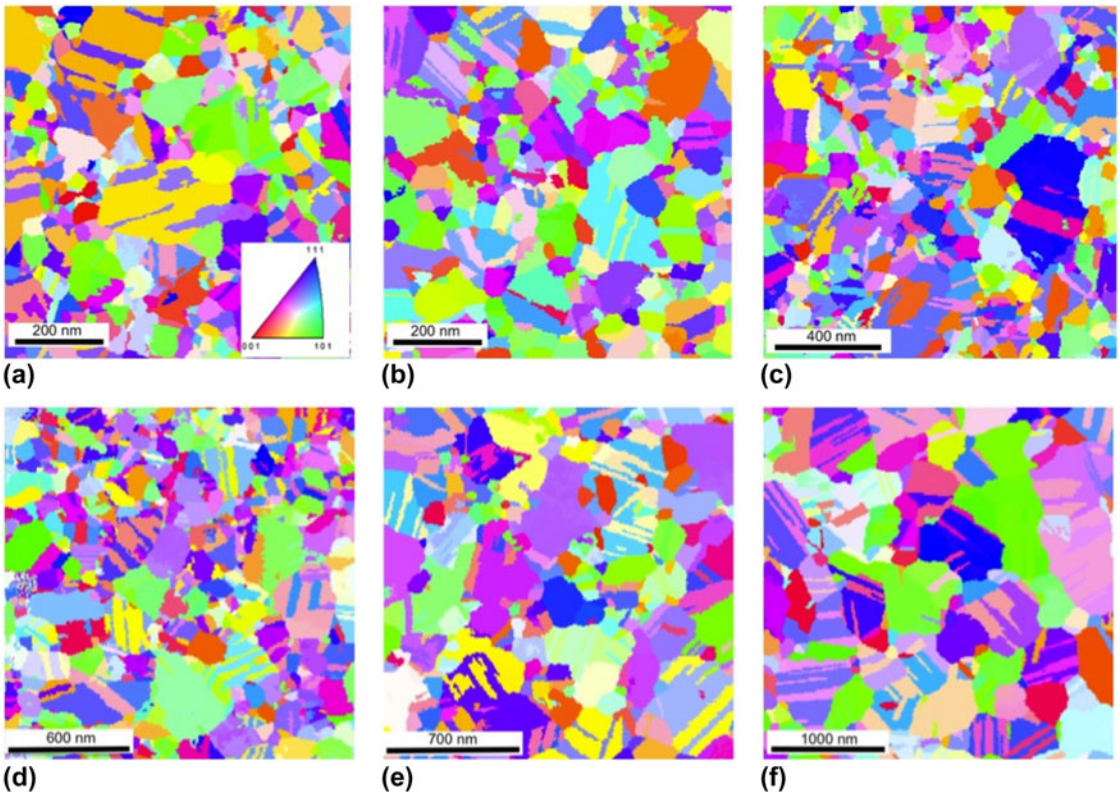

FIG. 2. Inverse pole figure maps in the sample normal direction for Cu/$Ta_{38}Si_{14}N_{48}$ films with film thicknesses of (a) 25.6 nm, (b) 38.2 nm, (c) 39.4 nm, (d) 56.8 nm, (e) 72.4 nm, and (f) 111.1 nm. Orientation of each grain can be determined from the color key in which [001], [101], and [111] are directions in the crystal reference frame.

average orientation to all pixels in a given grain. Finally, cleanup procedures were used to remove false grain boundaries created by 180° ambiguity. This particular type of misindexing occurs because of the similarity of diffraction patterns related to simple symmetry operations, e.g., 180° rotations along certain axes. False 180° boundaries with misorientation axes of 001, 101, 102, 103, 104, 105, 113, 114, 116, 117, 212, 213, 215, 223, 313, 314, 315, 317, 323, and 525 were removed with a tolerance angle of 1°. These cleanup procedures change only ~5% of the data points.

Grain boundary line segments were extracted from the orientation maps and used for calculating the GBCD. These line segments were reconstructed so that they deviated from true segments by no more than two pixels. More than 50,000 line segments were used for calculating the GBCD. Coherent and incoherent Σ3 boundaries were reconstructed with a misorientation tolerance angle of 9°. Coherent Σ3 boundaries were identified as twin boundaries whose boundary planes deviated from the {111} plane by no more than 8°. The choices of allowable misorientation and plane deviation are based on Brandon's criterion and are consistent with reported values.[37] Length fractions of total Σ3 and coherent Σ3 boundaries over the entire grain boundary population were calculated. After measurement of the Σ3 boundary length fraction, all Σ3 boundaries were excluded from the grain boundary network with a misorientation tolerance angle of 9° for grain size measurements excluding twin boundaries.

D. Influence of ASTAR™ scan step size on grain size measurement and boundary analysis results

As shown in Table II, different scan step sizes were used for collection of orientation maps. In this section, the influence of scan step size on grain size and Σ3 boundary length fraction measurements will be described. The sample Cu (72.4 nm)/$Ta_{38}Si_{14}N_{48}$ was chosen for the step size experiment. This sample has an ASTAR™ grain size of 147 nm. All grain size values in this paper are given as the equivalent circle diameter of the mean area. Six different scan step sizes ranging from 4 nm to 31 nm (1/40 to 1/5 of the mean grain size) were used to scan each field of view. The scan parameters are detailed in Table III. Table III shows that the number of points in the x and y directions was controlled so that each image had approximately the same field of view (1600 × 1600 nm). Figure 3 shows an example of boundary analysis results from the same area in the 72.4 nm-thick Cu sample

scanned using the six different step sizes. In Fig. 3, blue lines represent all Σ3 boundaries and red lines represent coherent Σ3 boundaries while black lines represent other grain boundary types. Grain size measurement and boundary analysis results of sample Cu (72.4 nm)/$Ta_{38}Si_{14}N_{48}$ scanned using the six different step sizes are shown in Table IV. Similar grain size measurement and boundary length fraction measurement results are obtained when scan step sizes ranging between 4 and 10 nm are used (Table IV). In contrast, boundary analysis results acquired with scan step sizes of 16 and 31 nm show large discrepancies from ones acquired with finer step sizes. This is a result of the inability of the coarser step sizes to capture the smaller grains, and hence the grain boundaries surrounding them. It is concluded that the choice of step size does not impact the experimental results as long as the step size used is between 1/40 and 1/15 of the mean grain size. In this work, all scan step sizes used for the six samples shown in Table II fall in this range. Therefore, the comparison of grain size and boundary fractions between different samples is not influenced by step size.

TABLE III. Scan parameters used for the evaluation of the impact of step size on twin length fraction and grain boundary character distribution. The sample used for these scans was Cu (72.4 nm)/$Ta_{38}Si_{14}N_{48}$.

Step size (nm)	Step size as fraction of average grain size	No. of points scanned
4	1/40	400 × 400
5	1/30	320 × 320
7.5	1/20	200 × 200
10	1/15	160 × 160
16	1/10	100 × 100
31	1/5	50 × 50

III. RESULTS AND DISCUSSION

A. GBCD of the Cu films

The relative areas of Σ3 grain boundaries, as a function of grain boundary plane orientation, for samples Cu (25.6 nm)/$Ta_{38}Si_{14}N_{48}$ and Cu (111.1 nm)/$Ta_{38}Si_{14}N_{48}$ are shown in Figs. 4(a) and 4(b), respectively. The relative areas reach a maximum at the coherent Σ3 positions. The values at the maxima as well as length fractions of all Σ3 and coherent Σ3 boundaries of the six films can be found in Table V. These distributions are consistent with Darbal et al.'s work on nanocrystalline Cu thin films.[20] It has been reported that grain boundary population and energy have an inverse correlation so that boundaries of

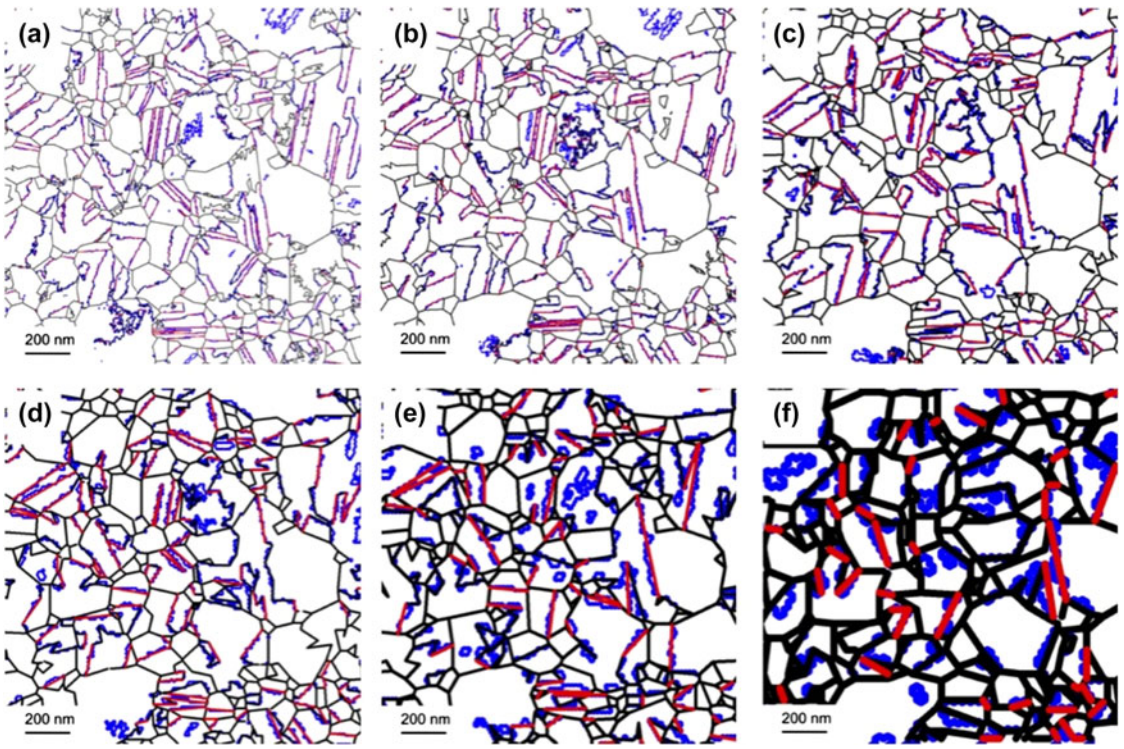

FIG. 3. Reconstructed boundary maps of the same area of Cu (72.4 nm)/$Ta_{38}Si_{14}N_{48}$ scanned using a step size of (a) 4 nm, (b) 5 nm, (c) 7.5 nm, (d) 10 nm, (e) 16 nm, and (f) 31 nm. In these maps, blue lines represent all twin boundaries and red lines represent coherent twin boundaries only while black lines represent other grain boundaries.

lower energy have higher populations.[38–40] As a result, coherent Σ3 boundaries, which have a lower boundary energy[41] compared to other grain boundary types, have a higher frequency in the Cu films. The low grain boundary energy of coherent twin boundaries can be explained by a low atomic misfit as well as by the broken bond model.[42] According to the broken bond model, surface energy reaches a minimum value at {111} planes for fcc materials.[42] Materials with a fcc crystal structure other than Cu also show a similar inverse correlation between energy and population as well as a high frequency at {111} planes.[43,44] As a comparison, recent measurements of the GBCD of body centered cubic (bcc) iron and tungsten show small relative areas for {111} planes.[24,45,46]

TABLE IV. Grain size measurement and boundary analysis results of sample Cu (72.4 nm)/$Ta_{38}Si_{14}N_{48}$ for different scan step sizes.

Step size (nm)	Grain size (nm)	Twin boundary length fraction (%)	Coherent twin boundary length fraction (%)	No. of boundary segments
4	147	48.2	23.2	76,224
5	149	47.8	24.6	60,534
7.5	145	47.0	24.2	31,957
10	148	45.6	22.9	25,096
16	146	41.6	18.0	20,321
31	150	33.9	12.2	12,065

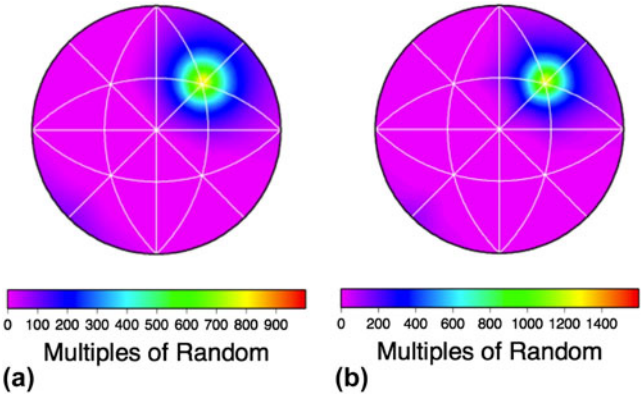

FIG. 4. The relative areas of grain boundaries with the Σ3 misorientation, plot on a stereographic projection along [001] of (a) sample Cu (25.6 nm)/$Ta_{38}Si_{14}N_{48}$ and (b) sample Cu (111.1 nm)/$Ta_{38}Si_{14}N_{48}$. The plots peak at the (111) position, corresponding to coherent Σ3 boundaries.

B. Increase in boundary length fraction with grain size

The measurements of the grain sizes and the length fractions of all Σ3 and coherent Σ3 boundaries of the six films are shown in Table V. The estimation of error for the boundary length fractions in Table V has been done by dividing the standard deviation of the measured length fraction from individual fields of views by the square root of the numbers of fields of views for each film. The relative area of the coherent twin as determined by the peak intensity of the GBCD for coherent Σ3, as well as the total Σ3 and coherent Σ3 length fractions directly measured from the orientation maps, are found to increase monotonically with grain size. In Fig. 5, the monotonic increase of the length fraction of coherent Σ3 boundaries with increasing grain size is plotted.

C. Twinning models in the literature

1. Gleiter's growth accident model

In 1969, Gleiter[25] proposed an atomistic model for the formation of annealing twins based on electron microscopic investigations of migrating grain boundaries and optical microscope measurement of twin density. In this model, twins are formed by a two-dimensional nucleation process on the {111} planes of the growing grain. Gleiter's model gives the following equation for the probability, p, of formation of a twin nucleus at a migrating boundary, which is also the probability for a {111} plane to be a twinning plane:

$$p = \exp\left\{\sigma_z\left(Q - kT\ln\frac{\Delta G^0}{kT}\right)\Big/\left[kT\sigma_z - \frac{\pi kT\varepsilon h^2}{\left(Q - kT\ln\frac{\Delta G^0}{kT}\right)}\right]\right\} . \quad (1)$$

In Eq. (1), Q is the activation energy for grain boundary migration, ΔG^0 is the difference in Gibbs free energy between the growing and the shrinking grain and is given by $\Delta G^0 = 4\delta\Omega/d$, where δ is the grain boundary energy,

TABLE V. Grain size measurement and boundary analysis results of the six Cu/$Ta_{38}Si_{14}N_{48}$ films. For twin boundary and coherent twin boundary length fractions, the error estimation is the standard deviation of the measured length fraction from individual fields of views divided by the square root of the numbers of fields of views for each film. For the grain size, the confidence interval at 95% confidence on the mean is given based on the measured population.[50]

Film thickness (nm)	25.6	38.2	39.4	56.8	72.4	111.1
Total twin boundary length fraction (%)	41 ± 1	43 ± 0.5	42 ± 0.6	44 ± 0.5	48 ± 0.7	53 ± 0.6
Coherent twin boundary length fraction (%)	18 ± 0.4	20 ± 0.3	21 ± 0.3	22 ± 0.3	24 ± 0.5	30 ± 0.8
GBCD intensity (MRD)	968	1158	1109	1180	1441	1570
No. of line segments	65,627	58,068	68,770	83,741	59,399	55,299
ASTAR grain size (nm)	51 ± 3	69 ± 3	87 ± 4	106 ± 5	147 ± 7	315 ± 16
No. of grains measured	4539	4297	1576	7997	4718	1256

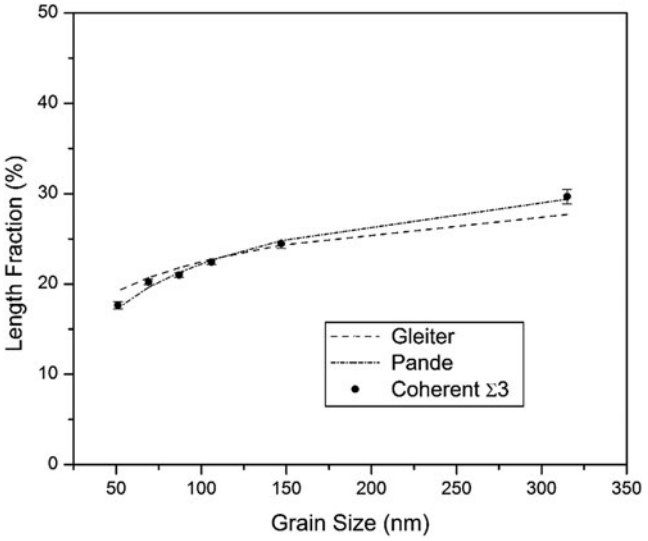

FIG. 5. Coherent Σ3 boundary length fractions are plotted as a function of grain size.

Ω is the atomic volume, and d is the grain diameter, σ_z is the energy of the coherent twin boundary, h is the height of the step formed by the twin nucleus (taken as the distance between {111} planes), ε is the energy of a step with height h, k_B is the Boltzmann constant, and T is the absolute temperature. The values of the parameters given by Gleiter are $Q = 3 \times 10^{-19}$ J/atom, $\sigma_z = 19.3$ mJ/m^2, $h = 2.087 \times 10^{-10}$ m, and $\varepsilon \approx \delta/2 = 315$ mJ/m^2. The value of Ω is calculated from the known lattice parameter and fcc structure of Cu as 1.1775×10^{-29} m^3.

In Gleiter's model,[25] a parameter p is given as the probability of formation of a coherent twin nucleus at a migrating grain boundary. However, in our experiments, coherent Σ3 boundaries are quantified in terms of length fraction of all grain boundary types. To relate p to the coherent Σ3 boundary length fraction, we proceed as follows. The probability p can be used to calculate the number of coherent twin boundaries per nanometer, as $T = p/h$ and the average number of expected coherent twin boundaries per grain, as $n = Td$, where the grain size d is taken as the equivalent circle diameter of mean area, $d_{<A>} = (4<A>/\pi)^{1/2}$, where $<A>$ is the mean area of grains. Assuming the average length of coherent twin boundaries to be equal to the mean chord length of a circle, i.e., equal to $\pi d_{<A>}/4$, then the fractional length of coherent Σ3 boundaries for the sample is given by the fractional length of the coherent Σ3 boundary per grain. This fraction can be calculated as the length of coherent Σ3 boundaries divided by the total length of boundaries, including coherent Σ3 boundaries, per grain:

$$l_{f\Sigma3} = \frac{\frac{n\pi d_{<A>}}{4}}{\pi d_{<A>} + \frac{n\pi d_{<A>}}{4}} = \frac{p d_{<A>}^2}{4hd_{<A>} + p d_{<A>}^2} \quad , \qquad (2)$$

where $\pi d_{<A>}$ is the perimeter of the (mean) grain. Note that in Gleiter's model, only the probability of the formation of coherent Σ3 boundaries is calculated. As a result, we distinguished between coherent and incoherent Σ3 boundaries and compared the length fraction of only coherent Σ3 boundaries to the fraction calculated from Gleiter's model.

In 2006, Li et al.[47] revisited Gleiter's model and proposed an updated set of values for the parameters in Eq. (1) based on more recent experimental data, while still providing good agreement between experimental and calculated results. For pure Cu, Li et al. proposed the following parameter set: $Q = 1.9 \times 10^{-19}$ J/atom, $\delta = 800$ mJ/m^2, $\sigma_z = 20.41$ mJ/m^2, and $\varepsilon = 400$ mJ/m^2 and found that this parameter set gives reasonably good agreement between the experimentally measured and the calculated results as a function of annealing temperature for a Cu sample with a grain diameter of 200 micrometers.

2. Pande's semiempirical model

Pande introduced a semiempirical model[33] in which the number of twins per grain, N, is given by

$$N = k\gamma_g \log D - k\gamma_g \log D_0 \quad , \qquad (3)$$

where k is a constant, γ_g is the grain boundary energy, D is the grain size, and D_0 is a critical grain size at or below which $N = 0$. A physical mechanism for this model was given in a later publication by Mahajan et al.,[26] which places Pande's model in the growth accident category.

In Pande's model,[33] the number of coherent twins per grain N is predicted, as shown in Eq. (3). N and $l_{f\Sigma3}$ can be related in a manner similar to that for Gleiter's model, taking again the grain size as the equivalent circle diameter of the mean area, $d_{<A>}$:

$$l_{f\Sigma3} = \frac{N\frac{\pi d_{<A>}}{4}}{\pi d_{<A>} + N\frac{\pi d_{<A>}}{4}} \quad . \qquad (4)$$

Rearrangement of Eq. (4) to obtain N using Eq. (2) gives:

$$N = 4l_{f\Sigma3}/(1 - l_{f\Sigma3}) = k\gamma_g \log d_{<A>} - k\gamma_g \log d_{<A>0} \quad . \qquad (5)$$

For the calculation of Pande's model, the number of coherent twins per grain, N, is calculated from Eq. (5)

using the coherent Σ3 length fraction values $l_{f\Sigma3}$, which are found in Table V. A plot of N versus log $d_{<A>}$ gives the slope and intercept as 1.045 and −0.946.

3. Grain encounter

The grain encounter theory states that grains, which are initially separated, touch each other during grain growth. If they happen to have a twin orientation, then the grain boundary will orient itself as a coherent twin boundary.[27–29,48] Burgers also proposes that the annealing twin density in fcc materials is dependent of the orientation relationship between the growing crystal and the matrix.[29]

D. Comparison between experimentally measured twin fractions to values calculated from physical models

Coherent Σ3 length fractions for the Cu films were calculated using Gleiter's and Pande's models [Eqs. (1)–(5)] and are plotted in Fig. 5. The model parameters used to plot the prediction of Gleiter's model, as determined by the lowest sum squared error (SSE), are those given by Li et al.,[47] except for the twin boundary energy σ_z, which is found to be 22.53 mJ/m^2. This value is about 10% higher than the value of 20.41 mJ/m^2 suggested by Li et al. A distinctive feature of the Cu films studied in the current paper is that they have the same thermal conditions, i.e., they were annealed at the same temperature for the same amount of time. Here, grain size and film thickness are considered to be the only independent variables while film thickness is not considered to be an influential factor for twin density in any models described in Sec. III. C. Therefore, as a comparison to Li et al.'s work[47] in which the temperature dependence of Gleiter's model was emphasized, the grain size dependence of Gleiter's model is evaluated in this paper.

Examination of Fig. 5 shows that both Gleiter's and Pande's models agree quite well with the experimental results. In other words, models for bulk, micron scale Cu work just as well for "nanoscale" Cu. Both models show a monotonic increase of coherent Σ3 length fraction with grain size. In Fig. 5, we are fitting the length fractions of coherent Σ3 boundaries only. Incoherent Σ3 boundaries are believed to form by a different mechanism and are therefore not considered in Gleiter's and Pande's models.

The growth textures of the six films are roughly the same as shown in Fig. 2. Based on the distribution of colors, the films are randomly textured. The orientation distribution of the six films will not be shown in this paper but is similar to the distribution of Darbal et al.'s nanocrystalline Cu films.[20] According to Warrington and Boon's work,[49] the fraction of Σ3 boundaries in a randomly textured film should be less than 2%. As a result, the grain encounter theory, as presented in Sec. III. 3, is ruled out as a possible mechanism to produce the large fraction of twins observed in these Cu films.

IV. CONCLUSIONS

In this work, a series of six Cu films with varying grain sizes and film thicknesses are studied via TEM based orientation mapping. The influence of scan step size on the measurement of all the Σ3 and the coherent Σ3 boundary length fraction was explored. It is found that the scan step size does not influence the grain size and boundary analysis results as long as it is 1/40–1/15 of the average grain size. GBCDs of the Cu films showed a maximum in relative area at the coherent Σ3 position, in agreement with previous reports on the GBCDs of fcc materials. 41–53% of grain boundaries in the Cu films are Σ3 boundaries while about half of the Σ3 boundaries are coherent.

Coherent Σ3 length fractions for the six Cu films were calculated and were shown to increase monotonically with grain size. The results were quantitatively compared to models for the formation of annealing twins. Both Gleiter's growth accident model and Pande's semiempirical model show good agreement with the results, allowing us to conclude that models for micron scale Cu work just as well for "nanoscale" Cu.

ACKNOWLEDGMENT

Financial support of the SRC, Task 1292.008 and 2121.001, and of the MRSEC program of the NSF under DMR-0520425 is gratefully acknowledged. G.S.R. acknowledges financial support from the ONR-MURI under the Grant No. N00014-11-1-0678. Portions of this research were carried out at the Stanford Synchrotron Radiation Lightsource, a Directorate of SLAC National Accelerator Laboratory, and an Office of Science User Facility operated for the U.S. Department of Energy Office of Science by Stanford University.

REFERENCES

1. T. Sun, B. Yao, A.P. Warren, K. Barmak, M.F. Toney, R.E. Peale, and K.R. Coffey: Surface and grain-boundary scattering in nanometric Cu films. *Phys. Rev. B* **81**, 155454 (2010).
2. L. Lu, Y.F. Shen, X.H. Chen, L.H. Qian, and K. Lu: Ultrahigh strength and high electrical conductivity in copper. *Science* **304**, 422 (2004).
3. P. Lin, G. Palumbo, U. Erb, and K. Aust: Influence of grain boundary character distribution on sensitization and intergranular corrosion of alloy 600. *Scr. Metall. Mater.* **33**, 1387 (1995).
4. S.B. Lee, T.S. Key, Z. Liang, R.E. Garcia, S. Wang, X. Tricoche, G.S. Rohrer, Y. Saito, C. Ito, and T. Tani: Microstructure design of lead-free piezoelectric ceramics. *J. Eur. Ceram. Soc.* **33**, 313 (2013).
5. T. Watanabe: An approach to grain boundary design for strong and ductile polycrystals. *Res Mech.* **11**, 47 (1984).

6. D. Field, L. Bradford, M. Nowell, and T. Lillo: The role of annealing twins during recrystallization of Cu. *Acta Mater.* **55**, 4233 (2007).
7. V. Randle: Twinning-related grain boundary engineering. *Acta Mater.* **52**, 4067 (2004).
8. K. Fuchs: The conductivity of thin metallic films according to the electron theory of metals. *Proc. Cambridge Philos. Soc.* **34**, 100 (1938).
9. Y. Shen, L. Lu, Q. Lu, Z. Jin, and K. Lu: Tensile properties of copper with nano-scale twins. *Scr. Mater.* **52**, 989 (2005).
10. O. Anderoglu, A. Misra, H. Wang, and X. Zhang: Thermal stability of sputtered Cu films with nanoscale growth twins. *J. Appl. Phys.* **103**, 094322 (2008).
11. K.C. Chen, W.W. Wu, C.N. Liao, L.J. Chen, and K.N. Tu: Observation of atomic diffusion at twin-modified grain boundaries in copper. *Science* **321**, 1066 (2008).
12. A.P. Sutton and R.W. Balluffi: *Interfaces in crystalline materials*. (Clarendon Press, New York, NY, 1995); pp. 2–95.
13. D. Xu, V. Sriram, V. Ozolins, J-M. Yang, K. Tu, G.R. Stafford, C. Beauchamp, I. Zienert, H. Geisler, and P. Hofmann: Nanotwin formation and its physical properties and effect on reliability of copper interconnects. *Microelectron. Eng.* **85**, 2155 (2008).
14. K. Kohama, K. Ito, T. Matsumoto, Y. Shirai, and M. Murakami: Role of Cu film texture in grain growth correlated with twin boundary formation. *Acta Mater.* **60**, 588 (2012).
15. N-J. Park and D. Field: Predicting thickness dependent twin boundary formation in sputtered Cu films. *Scr. Mater.* **54**, 999 (2006).
16. K. Pantleon, A. Gholinia, and M.A. Somers: Quantitative microstructure characterization of self-annealed copper films with electron backscatter diffraction. *Phys. Status Solidi A* **205**, 275 (2008).
17. E.F. Rauch and L. Dupuy: Rapid spot diffraction patterns identification through template matching. *Arch. Metall. Mater.* **50**, 87 (2005).
18. E.F. Rauch and M. Veron: Coupled microstructural observations and local texture measurements with an automated crystallographic orientation mapping tool attached to a tem. *Materialwiss. Werkstofftech.* **36**, 552 (2005).
19. E.F. Rauch, J. Portillo, S. Nicolopoulos, D. Bultreys, S. Rouvimov, and P. Moeck: Automated nanocrystal orientation and phase mapping in the transmission electron microscope on the basis of precession electron diffraction. *Z. Kristallogr.* **225**, 103 (2010).
20. A.D. Darbal, K.J. Ganesh, X. Liu, S.B. Lee, J. Ledonne, T. Sun, B. Yao, A.P. Warren, G.S. Rohrer, A.D. Rollett, P.J. Ferreira, K.R. Coffey, and K. Barmak: Grain boundary character distribution of nanocrystalline Cu thin films using stereological analysis of transmission electron microscope orientation maps. *Microsc. Microanal.* **19**, 111 (2013).
21. J.S. Carpenter, X. Liu, A. Darbal, N.T. Nuhfer, R.J. McCabe, S.C. Vogel, J.E. LeDonne, A.D. Rollett, K. Barmak, I.J. Beyerlein, and N.A. Mara: A comparison of texture results obtained using precession electron diffraction and neutron diffraction methods at diminishing length scales in ordered bimetallic nanolamellar composites. *Scr. Mater.* **67**, 336 (2012).
22. X. Liu, T. Nuhfer, J. Ledonne, S. Lee, A. Rollett, K. Barmak, J. Carpenter, and A. Darbal: Precession-assisted nanoscale phase and crystal orientation mapping of Cu-Nb composites in the transmission electron microscope. *Microsc. Microanal.* **18**, 1426 (2012).
23. X. Liu, N. Nuhfer, A. Rollett, S. Sinha, S-B. Lee, J. Carpenter, J. LeDonne, A. Darbal, and K. Barmak: Interfacial orientation and misorientation relationships in nanolamellar Cu/Nb composites using transmission-electron-microscope-based orientation and phase mapping. *Acta Mater.* **64**, 333 (2014).
24. X. Liu, D. Choi, H. Beladi, N.T. Nuhfer, G.S. Rohrer, and K. Barmak: The five parameter grain boundary character distribution of nanocrystalline tungsten. *Scr. Mater.* **69**, 413 (2013).
25. H. Gleiter: Formation of annealing twins. *Acta Metall.* **17**, 1421 (1969).
26. S. Mahajan, C. Pande, M. Imam, and B. Rath: Formation of annealing twins in fcc crystals. *Acta Mater.* **45**, 2633 (1997).
27. W. Burgers: Stimulation crystals and twin-formation in recrystallized aluminium. *Nature* **157**, 76 (1946).
28. W. Burgers: Crystal growth in the solid state (recrystallization). *Physica* **15**, 92 (1949).
29. W. Burgers, J. Meijs, and T. Tiedema: Frequency of annealing twins in copper crystals grown by recrystallization. *Acta Metall.* **1**, 75 (1953).
30. S. Dash and N. Brown: An investigation of the origin and growth of annealing twins. *Acta Metall.* **11**, 1067 (1963).
31. C.V. Kopezky, V.Y. Novikov, L. Fionova, and N. Bolshakova: Investigation of annealing twins in fcc metals. *Acta Metall.* **33**, 873 (1985).
32. C.V. Kopezky, A.V. Andreeva, and G.D. Sukhomlin: Multiple twinning and specific properties of sigma = 3N boundaries in FCC crystals. *Acta Metall. Mater.* **39**, 1603 (1991).
33. C. Pande, M. Imam, and B. Rath: Study of annealing twins in fcc metals and alloys. *Metall. Trans. A* **21**, 2891 (1990).
34. F. Chen and D. Gardner: Influence of line dimensions on the resistance of Cu interconnections. *IEEE Electron Device Lett.* **19**, 508 (1998).
35. T. Sun, B. Yao, A.P. Warren, V. Kumar, S. Roberts, K. Barmak, and K.R. Coffey: Classical size effect in oxide-encapsulated Cu thin films: Impact of grain boundaries versus surfaces on resistivity. *J. Vac. Sci. Technol., A* **26**, 605 (2008).
36. B. Yao, R.V. Petrova, R.R. Vanfleet, and K.R. Coffey: A modified back-etch method for preparation of plan-view high-resolution transmission electron microscopy samples. *J. Electron Microsc.* **55**, 209 (2006).
37. S.I. Wright and R.J. Larsen: Extracting twins from orientation imaging microscopy scan data. *J. Microsc.* **205**, 245 (2002).
38. G.S. Rohrer, D.M. Saylor, B. El-Dasher, B.L. Adams, A.D. Rollett, and P. Wynblatt: The distribution of internal interfaces in polycrystals. *Z. Metallkd.* **95**, 197 (2004).
39. K. Barmak, E. Eggeling, M. Emelianenko, Y. Epshteyn, D. Kinderlehrer, R. Sharp, and S. Ta'asan: Critical events, entropy, and the grain boundary character distribution. *Phys. Rev. B* **83**, 134117:1–12 (2011).
40. G.S. Rohrer: Grain boundary energy anisotropy: A review. *J. Mater. Sci.* **46**, 5881 (2011).
41. E.A. Holm, D.L. Olmsted, and S.M. Foiles: Comparing grain boundary energies in face-centered cubic metals: Al, Au, Cu and Ni. *Scr. Mater.* **63**, 905 (2010).
42. J.K. Mackenzie, A.J.W. Moore, and J.F. Nicholas: Bonds broken at atomically flat crystal surface—1: face-centered and body-centered cubic crystals. *J. Phys. Chem. Solids* **23**, 185 (1962).
43. G.S. Rohrer, E.A. Holm, A.D. Rollett, S.M. Foiles, J. Li, and D.L. Olmsted: Comparing calculated and measured grain boundary energies in nickel. *Acta Mater.* **58**, 5063 (2010).
44. E.A. Holm, G.S. Rohrer, S.M. Foiles, A.D. Rollett, H.M. Miller, and D.L. Olmsted: Validating computed grain boundary energies in fcc metals using the grain boundary character distribution. *Acta Mater.* **59**, 5250 (2011).
45. H. Beladi and G.S. Rohrer: The relative grain boundary area and energy distributions in a ferritic steel determined from three-dimensional electron backscatter diffraction maps. *Acta Mater.* **61**, 1404 (2013).

46. H. Beladi and G.S. Rohrer: The distribution of grain boundary planes in interstitial free steel. *Metall. Mater. Trans. A* **44A**, 115 (2013).
47. Q. Li, J.R. Cahoon, and N.L. Richards: On the calculation of annealing twin density. *Scr. Mater.* **55**, 1155 (2006).
48. M.A. Meyers and L.E. Murr: A model for the formation of annealing twins in FCC metals and alloys. *Acta Metall.* **26**, 951 (1978).
49. D.H. Warrington and M. Boon: Ordered structures in random grain-boundaries; some geometrical probabilities. *Acta Metall.* **23**, 599 (1975).
50. D.T. Carpenter, J.M. Rickman, and K. Barmak: A methodology for automated quantitative microstructural analysis of transmission electron micrographs. *J. Appl. Phys.* **84**, 5843 (1998).